J4.3 DEVELOPMENT OF AN AUTOMATED APPROACH FOR IDENTIFYING CONVECTIVE STORM TYPES USING REFLECTIVITY AND NEAR-STORM ENVIRONMENT DATA

Steven A. Lack[1*], and Neil I. Fox[2]
NOAA Earth Systems Research Laboratory, Boulder, CO
[1] Collaboration with the Cooperative Institute for Research in Environmental Sciences (CIRES), Boulder, CO

[2]University of Missouri-Columbia, Columbia, Missouri

1. INTRODUCTION

When examining precipitation systems with radar, many different types of objects may be identified. The simplest distinction between types of precipitation objects is the separation of convective from stratiform precipitation areas. Such automated classification procedures have been developed and employed by hydrometeorological users (e.g. Biggerstaff and Listemaa, 2000). In instances such as these, the primary motivation for identifying cells as convective or stratiform has been to improve estimates of rainfall rate from radar. Work has also been done to automate a process to distinguish simplified objects, linear versus cellular systems, given precipitation analyses (Stage IV data) (Baldwin et al. 2005). Both methods above provide a framework for improving quantitative precipitation forecasts (QPF) in some way and can give insight into mesoscale processes, but the process of identifying specific types of convective cells remains largely unexplored. The work herein provides a framework for an automated convective storm-cell classification algorithm, which includes linear convective systems, supercells, pulse thunderstorms and nonsevere/severe discrimination. The algorithm uses composite reflectivity data combined with near-storm environmental (NSE) data derived from the RUC-20 gathered from the WDSS-II system.

The identification and classification of storm cells in this framework is primarily aimed at adjusting life-cycle parameters in a nowcasting (0-2 hour forecast of reflectivity) framework. The underlying idea is that classifying a convective system and retaining information from prior time steps can lead to an understanding of growth, decay, and morphology of a particular storm. In particular this work is aimed at providing input parameters to constrain convective storm development and motion within a Bayesian hierarchical nowcast scheme such as ones described in Xu et al. (2005) and Fox and Wikle (2005). One may also choose to identify and classify convective storm elements for verification and climatological studies. This may be particularly useful in object-oriented verification procedures where matching objects from the truth to the forecast remains the biggest challenge.

*Corresponding author address: Steven A. Lack, 325 Broadway, NOAA, ESRL,GSD5, Boulder, CO, 80305
email: Steven.A.Lack@noaa.gov

2. WDSS-II

The WDSS-II system was used to a large degree for the data collection stage of the automated cell classifier and is described by Lakshmanan et al. (2007). The first set of data obtained for the classifier was Level-II radar data for a given radar site. The Level-II data have the highest spatial and temporal resolutions for current operational radar networks. Although the resolution of the radar data used is 1 degree (azimuth) by 1 km (gate spacing) a Cartesian transformation was applied to obtain data at a 1 km x 1 km resolution (w2merger: Lakshmanan et al. 2006). Although the merger algorithm in WDSS-II was primarily developed to merge multiple radars into one domain, merging data from a single radar results in a simple Cartesian grid of radar-derived variables. There are many merging strategies available within the algorithm and for this case the default exponential weighting scheme in space is used for interpolation. All elevation angles for the given data are merged resulting in constant altitude plan position indication (CAPPI) slices. From the CAPPI slices a composite radar image was created using the maximum reflectivity in a vertical column. This composite creation was chosen so that the product would maximize the rain rate for a given pixel, giving a worst-case scenario. This merging technique to a Cartesian grid allows for the data to be easily processed in future steps of the classification scheme.

As this work attempts to classify storm cells for use in determining growth, decay, maintenance, and morphology it is important to incorporate storm environment data as well. For the problem of forecasting storm longevity on the short (nowcasting) time scale, it was found that reflectivity alone cannot be used; however, with the inclusion of some environmental parameters forecasting trends of growth and decay may be possible (MacKeen et al. 1999). For the problem of incorporating the environmental data in a nowcasting time scale the Rapid Update Cycle at 20-km resolution (RUC-20) was considered the best solution as it has high spatial and temporal resolution and is used operationally. In addition, the WDSS-II suite readily ingests RUC-20 data and outputs gridded NSE data. Benjamin et al. (2002) provide details on the architecture and process of the RUC-20 model. It has been widely used in proximity sounding studies that focus on storm type and error characteristics of variables used from proximity soundings are relatively well known (Thompson et al. 2003).

WDSS-II readily ingests and converts RUC model grib files into fields used by the system to display basic fields of temperature, height, and pressure. From the basic fields, one can also run a near-storm environment algorithm which calculates parameters such as CAPE, SRH, CIN, and many other variables over different layers. For classification purposes, the storm environmental variables were calculated using the initialization data at the top of each hour for the duration of the event examined. The nearest radar time stamp was used to match the model data initialization to the reflectivity image. As an operational note, it may be necessary to run the identification of cells from forecast products from the RUC, as one needs to account for model issuance times. The combination of running the near-storm environment algorithm with the merging algorithm within WDSS-II results in a product with a resolution similar to the Cartesian product of reflectivity with the same domain.

3. IDENTIFICATION AND CLASSIFICATION OF CELLS

The identification of the individual storm cells was based on the object-oriented verification work from Micheas et al. (2007). In this framework, cells are identified based on a user-defined threshold of reflectivity (in this case 30 dBZ) and a minimum size threshold (in this case 40 km^2). A binary image is created for all pixels in the domain greater than the threshold. From this binary image, individual cells are identified if there is sufficient separation from their nearest neighbor. In other words, adjacent pixels within a cluster of reflectivity are tagged with the same cell identification number within the domain. The cell identification number ranges from 1 to the maximum cell number identified in the domain above the minimum size criteria. Once the cluster of pixels is identified as an individual storm cell and a number is assigned, storm attributes are derived for each cell in the domain. This is accomplished by overlaying matrices of near-storm environmental data and reflectivity-derived data to the matrix of identified cells. This results in storm attributes for each individually assigned storm cell within the given domain. For example, for a given identified cell, reflectivity, POH, CAPE, CIN, and SRH for all the pixels contained in the given cell are overlaid. From these data, values of maximum, minimum, and average (mean value) storm attributes are attained for all cells in the domain on which the cell classification will be based.

The overall objective was to use a classification tree to predict the membership of a certain object given its characteristics compared to a prior set of known classifications. Classification trees are useful in that they contain a hierarchical framework for working with data. Each step of the decision process for classification consists of what eventually turns out to be a series of “if else” statements branching from one initial decision (“root” node). The methodology consists of finding the best split possible at each node that results in the optimum-sized tree for deterministic classification. Classification and regression trees have been recently applied and have shown success in predicting lightning over the United States and Canada (Burrows 2007).

3.1 Expert Classification

In order to create a working dataset for classification, storm cells had to be identified individually and subjectively classified initially. The initial dataset consists of 15 different dates from 2004 to 2007 with over 360 individual identified cells covering various geographic regions; however, a majority came from the Midwest. The cases also span different seasons so that the classifier would be able to identify storm type independent on the time of year; however, cases deal only with warm precipitation (snow-producing storms are omitted). A majority of the cases also have severe storm reports associated with the given date. A severe report was not a necessity but allowed for dates and regions where convection was likely occurring to be easily identified.

A subjective “expert” classification of the individual convective storm cells commenced from the initial dataset. The expert classification followed a hierarchical procedure, starting with storm appearance in reflectivity imagery and continuing with derived radar products. These products included those from the storm cell identification and tracking (SCIT) algorithm (Johnson et al. 1998) contained in WDSS-II along with radar reflectivity- and velocity-derived products such as the hail detection algorithm (HDA: Witt et al. 1998) and the mesocyclone detection algorithm (MDA: Stumpf et al. 1998). Model data from the RUC-20 output run through the NSE algorithm in WDSS-II also provided additional information. An example of this expert classification involving a supercell requires the examination of the lowest available elevation scan for proper reflectivity structure (a possible hook), the detection of a mesocyclone from the MDA, strong probability of hail (POH) or severe hail (POSH), and a sheared environment with available potential energy that would support the claim of a supercell. The ultimate goal, in the case of the supercell, was to properly identify the possibility of a tilted, rotating updraft from the given data.

Eight different classification types were used in this study and are summarized in Table 1. An important distinction is made between air mass thunderstorms and pulse thunderstorms. Although similar in structure, the pulse thunderstorm has characteristics that allow for the rapid formation of hail and/or the possibility for a severe downburst. Also within the classification types, the two small-scale, rotating types may seem redundant; however, it was thought that significant differences may exist between severe and nonsevere varieties. The nonsevere variety may be thought of as an early stage or developing supercell while the severe variety may be more representative of a mini-supercell. These small-scale, rotating storm types have a slightly different physical makeup than the mature supercell. In addition, the severe versus nonsevere discriminator was used

Classification Types	Brief Description	Code
Air Mass Thunderstorm	Low Shear Environment	AM
Pulse Thunderstorm	Low Shear with Potential Severity	PULSE
Small-scale Rotating Thunderstorm	Organized Convection within Rotating Environment	SRT
Severe Small-scale Rotating Storms	Same as Above with High Reflectivity	SSRT
Linear Convective System	Squall-type System with Potential Severity	LCS
Linear Convective System (Rotation)	Squall-type System within Rotating Environment	LCSROT
Supercell	Severe Storm with Significant Rotation	SC
General Thunderstorm	Pre-frontal Non-severe and Other Convection	GEN T

Table 1. Eight classification types used within this classification tree study.

to potentially identify storms with the likelihood of carrying severe attributes throughout a majority of their lifecycle. This is useful information for nowcasting storm severity. In the expert classification process, the severe versus nonsevere discriminator was identified by using the Storm Prediction Center's (SPC) storm reports and the National Climatic Data Center's (NCDC) storm archives. In addition, maximum reflectivity signatures, the HDA, and the MDA were used in determining severe storms. The NSE fields produced by WDSS-II were again used to discriminate the potential for severe activity from organized convection with limited severe threat. This was essential in the case of discriminating between severe linear convective systems and general thunderstorms. General thunderstorms can take many forms as they are the left-over class. Often they are organized in a linear fashion along boundaries with weak forcing, which reinforces the need to use model data to aid in classification. Notice there is no severe versus nonsevere discriminator for supercells as this category implies a well-developed supercell that has significant potential for hail, damaging winds, and even tornadoes.

There is some inherent subjectivity to the division of the convective cells into eight categories. The categories themselves are relatively subjective as one may argue that there is some significant overlap of the divisions of convective cell types (i.e. supercell versus severe, small-scale rotating storm). Some of the subjectivity also pertains to storm reports or a lack thereof. Most of the classifications of storms into the severe category were based upon unofficial SPC storm reports. Note that report times do not always correspond to the actual events and that some reports are missed especially in the case of sparsely populated areas. During the expert classification process, storms without physical storm reports may be classified as severe based upon appropriate WDSS-II information. Fields such as probability of severe hail, maximum estimated hail size, as well as fields generated by the mesocyclone and tornadic vortex algorithm were used to supplement decisions in the classification process.

3.2 Classification Tree Structure

Once the storms were individually identified using expert classification, a table was generated complete with all storm attributes and tagged with one of the eight classification categories. From this information, a classification tree process was used to determine the optimum use of variables to automatically detect cell type. The classification process results in a tree of information with nodes at each branch representative of the best data split. These nodes have the advantage of yielding a probability that given certain criteria at a particular pruning stage that the identified cell belongs to a given class. The use of pruning to get probabilities of cell classification yields more meaningful results as it accounts for some degree of uncertainty in the classification; however, the tree eventually leads to a deterministic solution. The classification tree scheme will be briefly described below. For a more detailed review of creating and using classification trees, the reader is referred to Breiman et al. (1984).

Two splitting rules were available for use in this experiment: the Gini diversity index (GDI) and the twoing rule. The goal of the splitting rule is to make a split at a given node that minimizes the misclassification cost. In the case of GDI, we are interested in obtaining a measure of node impurity for splitting. Node impurity is given by (1), where $I(t)$ represents the impurity at node (t), f is the relative frequency of cases in t that belong to class c_j.

$$I(t) = 1 - \sum_{j=1}^{x} f(c_j, t)^2 \qquad (1)$$

This method involves a process that looks at which class to be categorized is largest. It then attempts to separate the classes by examining one class at a time. The mean squared error (MSE) is used to measure the performance of the classification tree for the GDI. For each class j, let c_j be an indicator variable that is 1 if the class for the example e is j and 0 otherwise; the MSE for this case is given by (2),

$$MSE = E_e\left[\sum_{j=1}^{x}(c_j(e) - P_j(e))^2\right] \qquad (2)$$

where the expectation (E_e) is over all examples, and $P_j(e)$ represents the probability assigned to class j for example e. The GDI minimizes the resubstitution estimate for the MSE. This is advantageous when

looking at unequal populations of events and is also the more efficient choice.

The twoing rule is different from the GDI in that the classes are selected so that half of the data is divided on each split. The result is a classification scheme that does not simply attempt to pull out one class initially, but pulls out the variable that maximizes the split into two equal populations.

The pruning technique inherent to classification trees is called minimal cost complexity pruning (Breiman et al. 1984). This process assumes that there is a linear increase in the bias of the resubstitution with the number of nodes for the tree. This cost (R_α) is assigned to a subtree and is composed of two terms including a resubstitution error for the given tree ($R(T)$) and the number of leaves (N) times a complexity factor α (3).

$$R_\alpha = R(T) + \alpha N \tag{3}$$

From the cost equation (3), a series of trees are created while varying α from 0 to infinity. These trees are nested and the tree that minimizes the overall cost is selected to represent the group.

Overall, the GDI method to grow classification trees involves four steps. The first uses (1) to calculate the diversity index on the parent node. The second step calculates the resultant GDI for the two child nodes from the split at the parent node. Weights are then arranged according to the proportion of the parent node in each child. Lastly, an improvement measure is calculated by minimizing the cost from each created subtree.

Input into the tree growth algorithm includes a matrix of a series of variables each having a known classification. Again, the classification was broken down into eight convective cell types. The reflectivity-derived and near-storm environmental variables were limited by availability in the WDSS-II scheme but follow closely with research previously done using proximity soundings with RUC-20 data (Thompson et al. 2003; Coniglio et al. 2006; Cohen et al. 2006). A training set was created from the input variables and the known classification. The results of the training and classification will be found in section 4.

3.3. Identification Example

The example for the cell classification was the severe weather outbreak over Missouri on 12 March 2006. The time period selected for this example was 2200UTC (Figure 1). The domain for the radar image was centered over the KEAX radar site and extends over a256 x 256 km area. The radar image was created using a maximum composite scheme and then run through the cell identification scheme.

Figure 1. The maximum composite reflectivity image from 12 March 2006 centered over the KEAX radar site at 2200UTC.

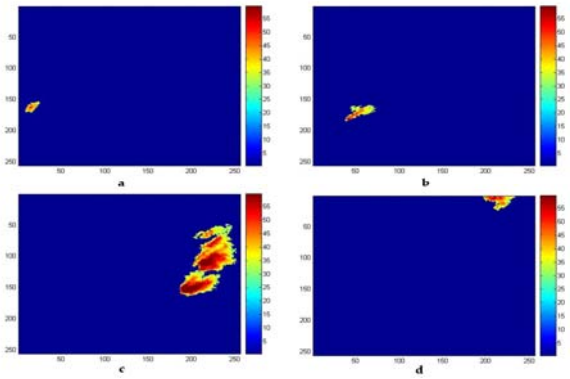

Figure 2. The identified cells from 12 March 2006 composite reflectivity centered over the KEAX radar site at 2200UTC. Four distinct objects were identified in this particular case with each cell labeled a-d.

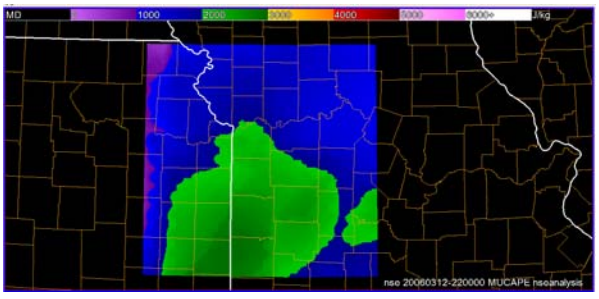

Figure 3. The MUCAPE field from 12 March 2006 centered over the KEAX radar site at 2200UTC. At this time, MUCAPE is weakening to values less than 3000 Jkg^{-1}.

Figure 1 shows the identification of the different cells in the domain after they have been isolated at the 30-dBZ threshold and have passed the minimum size criterion (>40 km^2). In Figure 2 multiple supercells are identified as one cluster of supercells, this occurs as enough

12 March 2006 at 2200UTC Cell Array				
SIZE	3641	459	403	162
MAXREF	73.704	57.000	58.869	51.000
STDREF	10.058	7.039	6.359	4.938
ECHOZ	50081	41409	42962	36631
VIL	67.173	26.577	15.656	7.695
SRH	613.64	740.08	226.56	191.37
MUCAPE	1516.9	1322.8	2205.2	1327.9
DCAPE	800.73	11.17	825.69	746.17
AVGVGP	0.435	0.494	0.448	0.382
EHI	5.743	6.118	3.122	1.594
SHEAR	44.327	44.920	37.329	41.165
RH_LCL	78.634	97.904	70.539	58.252
RATIO	2.833	1.744	2.553	2.331
MU/SBCAPE	1.993	1322.8	1.636	1.143
ROT "EXPERT" TYPE	TVS Meso Supercell Cluster	Circ Decaying Supercell	Circ Growing Rotating Storm	Circ Growing Rotating Storm

Table 2. Selected output fields for the 12 March 2006 case at 2200 UTC including the "expert" classification, for units and category descriptions see Table 1.

overlap of the 30-dBZ regions is present. The scheme dictates that as long as a part of the cluster contains supercell characteristics, the entire identified cell will be considered a supercell.

Once the individual cells are tagged with identifying numbers, the algorithm calculates and overlays reflectivity-derived parameters along with selected NSE variables derived from the RUC-20 via the WDSS-II software. Figure 3 shows an example of the most unstable CAPE (MUCAPE) field that was overlaid on the composite reflectivity field, while Figure 4 shows the MUVGP and Figure 5 shows the SRH in the 0 to 3-km layer. These figures illustrate the variability in a small domain (256 x 256 km) at a 20-km resolution. Significant changes in these variables over such short distances can alter the evolution of the individually tagged storm from Figure 2. For each time, a table of storm attributes is created including the reflectivity-derived and the NSE variables which will be input into the classification tree. Table 2 includes some of the selected fields used for classification for the 12 March 2006 example from Figure 2. Accompanying the selected variables is the subjective "expert" classification that will fall into one of the eight classifications from Table 1 for input into the classification tree routine.

4. CLASSIFICATION EXPERIMENTS

There were four experiments conducted which used different training sets yielding different resultant classification trees. Two of the experiments will be detailed in this paper including a training set consisting of reflectivity-derived fields only and a training set consisting of reflectivity-derived fields coupled with near-storm environmental parameters.

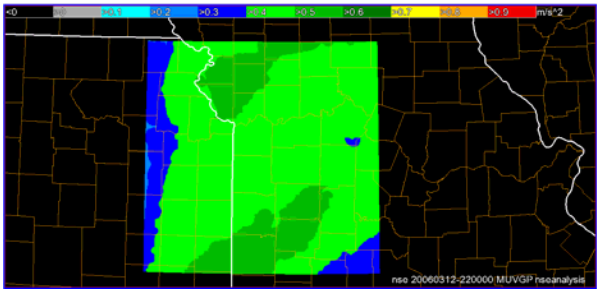

Figure 4. The MUVGP field from 12 March 2006 centered over the KEAX radar site at 2200UTC. Notice values exceeding 0.3 ms^{-2} throughout the domain which signifies the continuing threat for rotating storms.

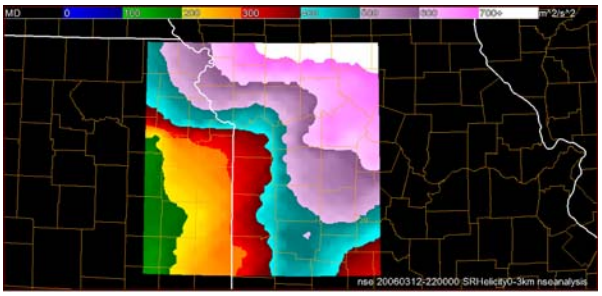

Figure 5. The MUVGP field from 12 March 2006 centered over the KEAX radar site at 2200UTC. Notice values exceeding 0.3 ms^{-2} throughout the domain which signifies the continuing threat for rotating storms.

4.1. Reflectivity-derived Fields Only

The classification tree used for this study first tests the hypothesis from MacKeen et al. (1999) that using reflectivity data alone does not provide the necessary information for predicting storm longevity. The tree is created using information on reflectivity-derived products and shape information. Reflectivity-derived products include: maximum reflectivity, mean reflectivity, the standard deviation of reflectivity, vertically integrated liquid (VIL), VIL density, probability of severe hail (POSH), and maximum estimated hail size (MESH). The shape parameters include the echo top height, the aspect ratio of the storm, and the storm size.

Equal populations, 16 of each storm type, were used in the creation process. Figure 6 shows the classification tree using reflectivity data only. Figure 7 shows the misclassification costs which correspond to the number of terminal nodes created by the tree. It is notably best to prune the reflectivity only tree at the point corresponding to where the lowest cross-validation error occurs. For this case, that level is 5, and the cross-validation error is 0.4833. It is interesting to note that using linear classification yields a cost of 1.0333. Clearly, using reflectivity only to create a decision tree fails when using linear classification methods.

For the end node that results in the supercell classification, the size range was 745 to 3013 km^2, the mean VIL density was greater than 2.15 g m^{-3}, the maximum reflectivity was greater than 60.08 dBZ, and the aspect ratio was less than 3.2. The aspect ratio being less than 3.2 reveals that the storm should appear more circular in nature which agrees with the supercell structure. The intense reflectivity and size range also coincide with most supercell observations. From the supercell end node, estimated probabilities of the eight storm types are given and can be incorporated into an automated procedure (neural network) for classification.

Upon further examination of the classification tree using reflectivity-derived products only, it is apparent that there are a few problems with the logic used to create a few of the branches in the testing phase. The main issue stems from the frequency of using maximum reflectivity for splitting; an example is found at the first two nodes on the left side of the tree in Figure 6. The first split using a maximum reflectivity of 51.175 should result in a separation of severe and nonsevere events; however, an examination of the final nodes shows that nonsevere storms are still classified with size becoming the main discriminating factor. Distinguishing between small storms using storm size does not make intuitive sense as the smaller scale storms (from Table 1) should have approximately the same size. In addition to the overuse of maximum reflectivity there seems to be improper splitting at the end of the tree in the discrimination between linear convective systems and supercells. The aspect ratio is used in this case and the classification results in a supercell if the ratio is greater than 1.40425. Clearly a linear convective system should have a greater aspect ratio and some considerable misclassification is occurring. Finally, the tree does not seem to have an ideal pruning level; the eight classification types do not appear uniquely at one pruning level as is shown when combining RUC-20 data and radar-derived fields.

Once the training phase is complete using equal populations and reflectivity-derived fields only, additional cases are put into the scheme and the created tree classifies the new and complete data set using all storms. At this point the quality of the tree can be assessed. Information from other identified cells from various dates and geographic locations may be used with the same reflectivity-derived data set used as input to the classifier. Once the new data set is run through the scheme, the deterministic classification from the test tree is compared with the expert classification. The first comparison is an exact-match approach where the deterministic classification from the tree must match the expert classification exactly. The second comparison made allows for adjustments to the match as long as the match is deemed not to be a total miss in classification. For example, for an event to be classified by the tree as a supercell but for which the “expert” classification reveals a severe, small-scale, rotating storm, the case is flagged as a match instead of a nonmatch as the classification is close to the truth and would not prove to be a problem operationally. However, for the case of a linear convective system with rotation being matched to a pulse thunderstorm, this would still be considered a mismatch.

In the case of using reflectivity data only to create the classification tree, the exact classification rate from 365 cells including the training cells was 0.417, while the marginal classification rate of those same cells was 0.618. Table 3 shows a breakdown of skill scores including POD, FAR, and CSI for the eight classification types for exact matches. Generally, the classification rates of success are not as high as desired when using reflectivity-derived products only; this coincides with the observations made by MacKeen et al. (1999).

A contingency table for each of the eight storm classifications for exact matches using reflectivity-derived products only is shown in Table 4. The table was created using 365 expert classification observations and the resulting classification from the decision tree. Values should be maximized along the diagonal of the table for optimal performance. . Outliers are readily apparent when examining the table, especially when examining the severe, small-scale rotating storm (SSRS) and the nonsevere, small-scale rotating storm (SRS). These outliers are mirrored in the pulse and air mass storm classifications as well. From the table it is also clear which storm types are being over- or under-classified. For example, there are a total of 62 observed supercells and only 34 are accurately classified for the reflectivity-derived product only tree. Overall, it is evident that distinguishing between larger-scale storms using reflectivity-derived products alone is a weakness.

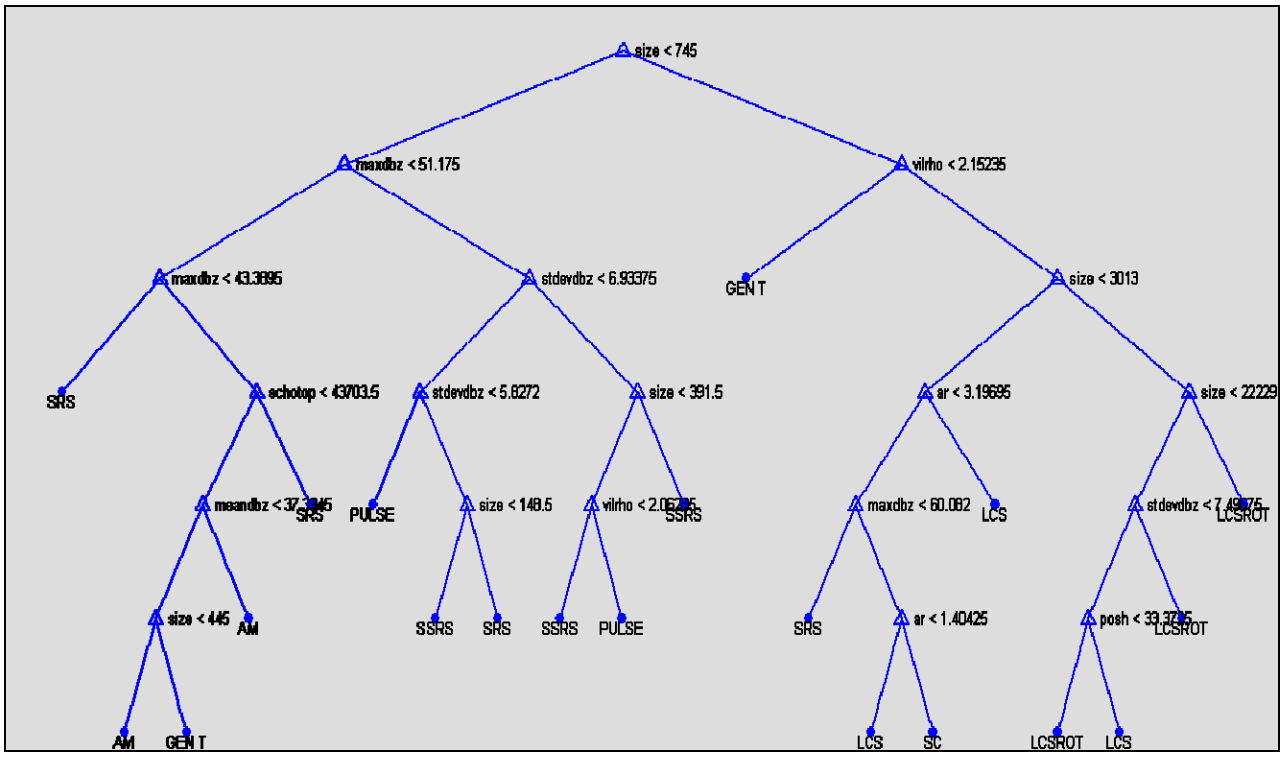

Figure 6. The cell classification tree using reflectivity only.

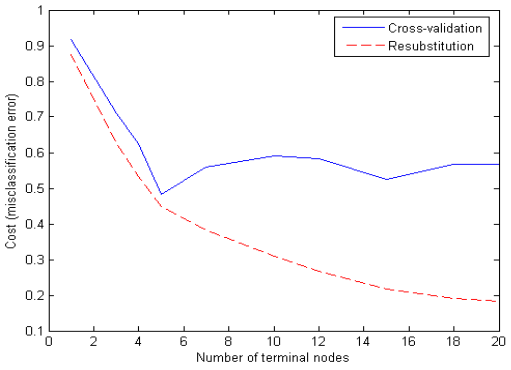

Figure 7. The misclassification error (cost) for the classification tree using reflectivity-derived products only. The resubstitution error is an idealized cost where the cross-validation curve shows the actual cost for the different terminal nodes.

4.2 Adding NSE Fields

The advantage of the tree classification scheme is that large datasets may be used to construct the ideal-sized (pruned) tree. There is not an immediate necessity to select certain RUC-20 fields for use in the classification tree formulation. The scheme itself will select the best splits at each node given the large data array by the methods described in section 3.2. This allows for easy comparison between previous studies on near-storm environmental fields for certain convective storms and the fields identified for use in the classification tree scheme.

Standard Skill Scores (Exact Match)			
Storm Type	**POD**	**FAR**	**CSI**
Supercell	0.317	0.412	0.260
Linear Convective System	0.370	0.706	0.196
Linear Convective System with Rotation	0.321	0.591	0.220
Small Rotating Storm	0.240	0.765	0.135
Severe Small Rotating Storm	0.389	0.548	0.264
Pulse	0.385	0.753	0.177
Air Mass	0.600	0.580	0.328
General Thunderstorm	0.550	0.333	0.431

Table 3. Skill scores for exact matches for the classification tree using reflectivity-derived parameters only.

	SC	SSRS	SRS	LCS	LCSROT	AM	PULSE	GEN T	Total Obs
SC	20	10	2	14	8	0	5	3	62
SSRS	3	28	8	0	0	1	29	2	71
SRS	0	3	12	0	0	26	9	0	50
LCS	4	0	4	10	5	0	1	3	27
LCSROT	5	3	1	8	9	0	1	1	28
AM	0	2	3	0	0	21	9	0	35
PULSE	2	16	10	1	0	2	20	1	52
GEN T	0	0	11	1	0	0	6	22	40
Total Class	34	62	51	34	22	50	80	32	365

Table 4. Contingency table for the expert-classified observation cell types (x-axis) and the output from the reflectivity-derived products only decision tree. The table was created for 365 total cells.

The classification tree created using fields created by the WDSS-II NSE algorithm using RUC-20 data should provide better results than when using reflectivity products alone. The tree created when using the combination of radar reflectivity-derived fields along with RUC-20 NSE fields is shown pruned to the eight classification types in Figure 8. The misclassification errors (cost) at each terminal node are shown in Figure 9. The cross-validation cost of the tree at the pruned level shown in Figure 8 is at a minimum (0.275). When doing a linear classification, the cost drops to around 0.125; however, more work would need to be done to examine the full effectiveness of a linear classification tool in this seemingly nonlinear application. The supercell classification end node shown in Figure 8 reveals that the supercell classification relies on a mean VGP to be greater than 0.299 ms^{-2} and a size between 745 and 3734 km^2. The VGP value is consistent with the findings by Thompson et al. (2003) for supercells utilizing RUC proximity soundings. Note that for the classification tree using RUC data and reflectivity-derived products, the main split uses the VGP and separates the tree into the four nonrotating storm types and the four rotating storm types. Physically this is a logical first split. The addition of some kind of model-derived rotation quantity alone improves the formulation of the classification tree(s).

From the exact comparison, the tree using RUC-20 fields with the radar-derived fields yields a classification success rate of 0.50. When accounting for near matches this figure jumps to 0.78. When examining standard skill scores for the eight different types of storms for exact matches (Table 5) and for near matches (not shown) an improvement is evident in comparison with the reflectivity-derived parameters only classification tree. It is important to keep in mind that in the success rate comparison, deterministic classifications are used. If the estimated probabilities, or misclassification rates were used, more insight into the success of the classification scheme could be attained.

Standard Skill Scores (Exact Match)			
Storm Type	**POD**	**FAR**	**CSI**
Supercell	0.556	0.300	0.449
Linear Convective System	0.778	0.447	0.477
Linear Convective System with Rotation	0.071	0.600	0.065
Small Rotating Storm	0.720	0.478	0.434
Severe Small Rotating Storm	0.333	0.467	0.258
Pulse	0.269	0.600	0.192
Air Mass	0.400	0.754	0.179
General Thunderstorm	0.750	0.565	0.380

Table 5. Skill scores for exact matches for the classification tree using an even population of reflectivity-derived parameters combined with near - storm environmental data from the RUC-20 model.

When examining where problems exist within the classification scheme, it becomes evident that the small-scale convective cells and some of the linear type of storms are frequently misclassified. However, upon examination of the small-scale systems, the node splits are consistent with observations. For example, the standard deviation of reflectivity is used to discriminate between severe and nonsevere storm types. The standard deviation is a way of examining maximum reflectivity gradients. In the case of small-scale severe storms, this gradient should be large when viewing composite reflectivity as this would represent a nearly vertical updraft supporting large hail. The problem in the small-scale storms may exist with the expert classification. Comparisons of storms with hail reports and storms of similar structure with no hail reports may need to be made for an accurate subjective classification. Objects that are similar in overall structure but do not produce observable severe weather still need to be grouped in the same category.

A contingency table for each of the eight classifications for exact matches is shown in Table 6, highlighting some of the strengths and weaknesses of using the combination of RUC-20 data with the radar reflectivity-derived products. Overall, there is vast improvement in discriminating between rotating and nonrotating types with the addition of RUC-20 data; however, work still needs to be done on the smaller-scale storms.

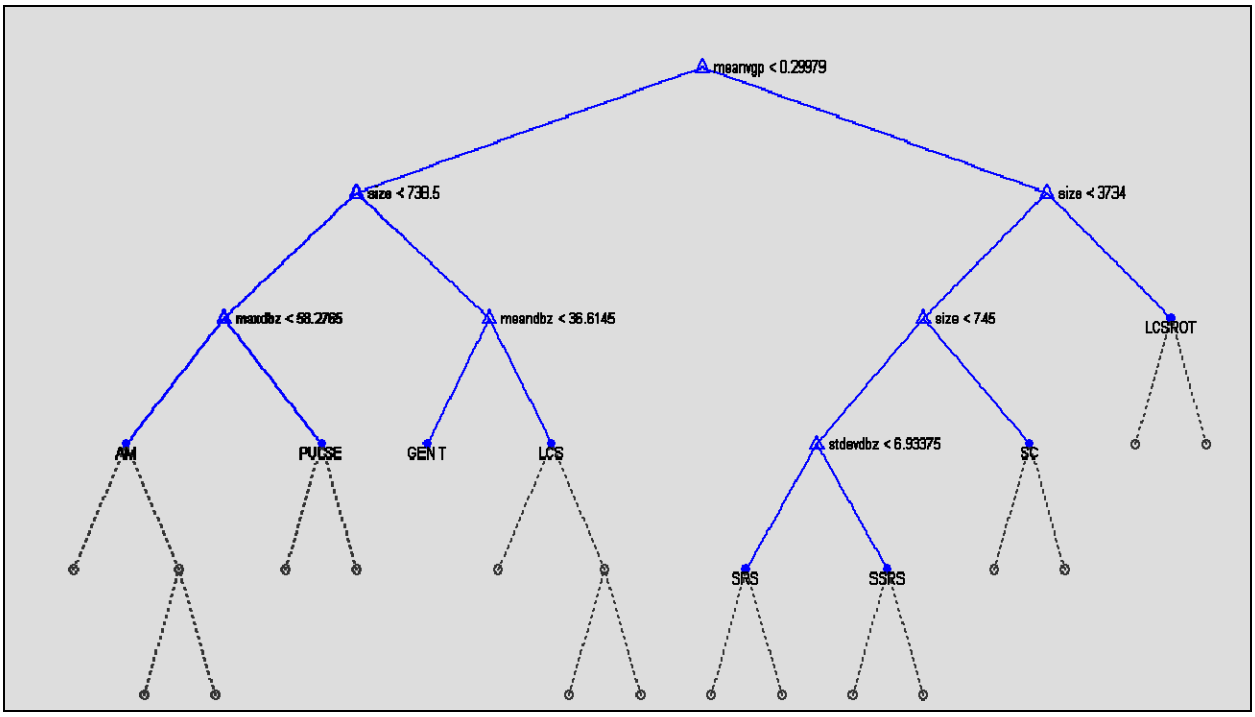

Figure 8. Classification tree for the RUC-20 fields combined with reflectivity data calculated from the WDSS-II system. The tree is pruned at level 2 of 8 to capture the eight classification types at the end nodes.

	SC	SSRS	SRS	LCS	LCSROT	AM	PULSE	GEN T	Total Obs
SC	34	17	2	3	1	0	0	5	62
SSRS	3	24	19	0	0	7	14	4	71
SRS	0	1	36	0	0	11	1	1	50
LCS	0	0	0	21	2	1	2	1	27
LCSROT	11	0	0	10	2	0	0	5	28
AM	0	1	3	0	0	14	4	13	35
PULSE	0	2	4	2	0	20	14	10	52
GEN T	0	0	4	2	0	4	0	30	40
Total Class	48	45	68	38	5	57	35	69	365

Table 6. Contingency table for the expert classified observation cell types (x-axis) and the output from the even population RUC-20 model fields combined with reflectivity-derived products decision tree. The table was created for 365 total cells.

5. CONCLUSIONS

For the nowcasting problem, the information needed to capture growth, decay and morphology is encapsulated in the eight classifications described in previous sections. This does not include the many sub-types of supercells and linear convective systems (squall lines) that may appear in the literature. For the research herein, the focus is primarily on the type of weather produced by the different storm types. We assumed that the different types of linear convective systems produce high winds on many occasions, and that the subtypes of supercells all have the potential to produce hail and damaging winds. This research attempts to categorize smaller types of cells such as the pulse, air-mass, and small rotating storms, and this can be understood from the stand point of lifecycles. For example, an air mass storm is more likely to have a shorter residence time than a small rotating storm which may evolve into a supercell or at least persist for a longer time.

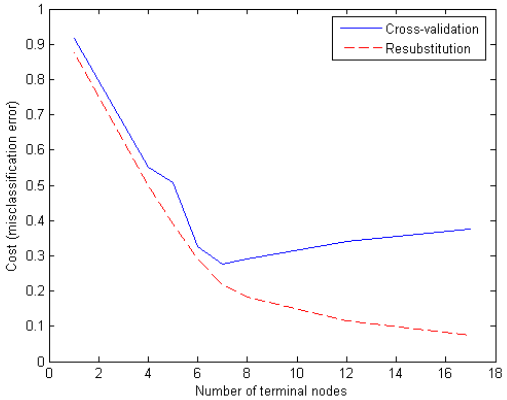

Figure 9. The misclassification error (cost) for the classification tree using an even population with reflectivity-derived products combined with RUC-20 NSE fields. The resubstitution error is an idealized cost where the cross-validation curve shows the actual cost for the different terminal nodes.

Furthermore, the air mass to pulse discrimination results in the prediction of severe weather reports. Pulse thunderstorms tend to have strong updrafts capable of producing hail or strong downbursts. These smaller types of storms have been shown to be difficult to classify due to the nature of their short persistence times and deficient information of the three-dimensional structure of the updraft or suspended higher reflectivity cores. It may therefore be concluded that with the lack of three-dimensional information (updraft orientation and height of maximum reflectivity), it may only be useful to separate the rotating, small-scale storms from the nonrotating, small-scale storms instead of including an attempt to distinguish between severe or nonsevere.

Potential uses of the classification include informing an object-oriented nowcast scheme on how to evolve the shapes in space and how to grow and decay them based on trends found in the model and trends found in the reflectivity fields. For nowcasts made further than 60 minutes, a RUC-20 forecast solution may be used to predict future classification of the identified cell. The incorporation of RUC-20 data at forecast times, instead of the initial time, may introduce more error to the nowcast system, but allows the classification to still have some of its roots in the general reflectivity structure of the given identifiable storm.

Trends in the classification over time can also be used to provide insight into the storm's life cycle. This requires some consistency in the observation; however, storm splits and mergers may be able to be handled well with the increase or decrease in observed cells and their corresponding properties used in the classification process. These trends may also be used to pick out time steps that may have been misclassified due to poor model initialization or gaps in radar data.

MCS longevity studies (i.e. Coniglio et al. 2006) indicate the possibility of using model fields for the nowcast problem. The research herein takes this a step further by breaking down longevity based on individual cells instead of entire regions. Note also that the occurrence of the storm cells in the domain may alter the environment, thus making it important to evaluate storm cells on a case-by-case basis. Finally, it may be useful for future derivations of the storm classifier to use only the model fields utilized for MCS maintenance outlined by Coniglio et al. (2006). This may yield better and physically more realistic results than allowing the tree classification creation scheme to select from a large data set.

6. FUTURE WORK

Future work with the cell classification problem includes a large-scale effort to develop an expert classification database that would require continuous updating. This database would be instrumental in the setup of a neural network. For a given date, cases must be selected that exhibit cells that have a pure classification in one of the eight categories. Further research may also be conducted on decreasing the number of cell types. It may be useful to reduce the number of classification types to six. This would result in removing the severe versus nonsevere type of small-scale convection. Combining the air-mass thunderstorm with the pulse thunderstorm along with combining the two smaller-scales, rotating thunderstorms may be essential to improving classification until more three-dimensional fields can be used in a near-real time setting. Alternatively, there is the possibility of an increase in storm categories if it is determined there are more then eight life-cycle models that should be applied in the nowcasting problem. Overall, the first step in future work of the classifier should be to create a large database of ideal storm classes to be used in the problem.

The use of velocity products from Level-II radar data may give some insight for the storm classification problem. Currently, there are products that can be displayed in the WDSS-II software package which include azimuthal shear and divergence derived from Doppler velocities. The fields appear in regions of significant reflectivity, including ground clutter. From the azimuthal shear product for the lowest elevation angle (0.5°), it can be shown that for areas of significant rotation, there is a peak in azimuthal shear values. Also, at the lowest elevation angle significant rotation appears to be found near a couplet of strong divergence and convergence upon examining the divergence product. The utility of these fields in the classifier may be assessed in the near future.

Enhancements of storm identification for the classification experiment may also be needed. Storm cells that are merging or splitting may cause a problem for identification. This can be avoided by using a multi-Doppler radar analysis to calculate updraft motions in the storms (Stalker and Knupp, 2002). From the identification of significant updrafts, storms may be readily identified as being separate entities in the splitting/merging stages of development or morphology. This process will remain a problem in the immediate future as multi-Doppler analysis is only available during research and in a few select regions that may have significant radar coverage overlap.

Finally, a number of other methodologies can be applied in place of the classification tree used in this research. Substituting a Bayesian Additive Regressive Tree (BART: Chipman et al. (2005) may result in better estimations on the probabilities of proper classification of the expert storm types. This method is relatively new and has shown vast improvements over standard classification and regression trees of the past. A comparison between the linear Fisher discriminant (LFD) and the nonlinear kernel Fisher discriminant (KFD) with the classification tree methodology might also show interesting results in classifying convective storm types.

7. REFERENCES

Baldwin, M.E., J.S. Kain, and S. Lakshmivarahan, 2005: Development of an Automated Classification Procedure for Rainfall Systems. *Mon. Wea. Rev.*, **133**, 844-862.

Benjamin, S.G., G. Grell, S. Weygandt, T. Smith, T. Smirnova, B. Schwartz, D. Kim, D. Devenyi, K. Brundage, J. Brown, G. Manikin, R. Peterson, 2002: RUC20—The 20-km version of the Rapid Update Cycle. NOAA Tech. Memo. OAR FSL twentyeight. Forecast Systems Laboratory, Boulder, CO, 9 pp.

Biggerstaff, M.I. and S.A. Listemaa, 2000: An improved scheme for convective/stratiform echo classification using radar reflectivity. *J. Appl. Meteor.*, **39**, 2129–2150.

Breiman, L., J.H. Friedman, R.A. Olshen, and C.J. Stone, 1984: Classification and Regression Trees. Chapman and Hall, pp. 358.

Burrows, W.R., 2007: Dynamical-statistical models for lightning prediction to 48-hr over Canada and the United States. *Preprints: 5th Conference on Artificial Intelligence Applications to Environmental Science, San Antonio, TX.*

Chipman, H.A., E.I. George, and R.E. McCulloch, 2005: BART: Bayesian Additive Regression Trees. Technical Report.

Cohen, A.E., M.C. Coniglio, S.F. Corfidi, and S.J. Corfidi, 2006: Discrimination of mesoscale convective system environments using sounding observations. *Preprints: 23rd Conference on Severe Local Storms, St. Louis, MO.*

Coniglio, M.C., M. Bardon, K. Virts, and S.J. Weiss, 2006; Forecasting the maintenance of mesoscale convective systems. *Preprints: 23rd Conference on Severe Local Storms, St. Louis, MO.*

Fox, N.I., and C.K. Wikle, 2005: A Bayesian Quantitative Precipitation Nowcast Scheme. *Wea. Forecasting*, **20**, 264–275.

Johnson, J. T., P. L. MacKeen, A. E. Witt, E. D. Mitchell, G. J. Stumpf, M. D. Eilts, and K. W. Thomas, 1998: The storm cell identification and tracking algorithm: An enhanced WSR-88D algorithm. *Wea. Forecasting,* **13**, 263–276.

Lakshmanan, V., T. Smith, K. Hondl, G. J. Stumpf, and A. Witt, 2006: A real-time, three dimensional, rapidly updating, heterogeneous radar merger technique for reflectivity, velocity and derived products. *Wea. Forecasting*, **21**, 802-823.

Lakshmanan, V., T. Smith, G. J. Stumpf, and K. Hondl, 2007: The warning decision support system - integrated information (WDSS-II). *Wea. Forecasting*, **22**, 596-612.

MacKeen, P.L., H.E. Brooks, and K.L. Elmore, 1999: Radar reflectivity-derived thunderstorm parameters applied to storm longevity forecasting. *Wea. Forecasting*, **14**, 289-295.

Micheas, A., N.I. Fox, S.A. Lack, and C.K. Wikle, 2007: Cell identification and verification of QPF ensembles using shape analysis techniques. *J. Hydrology, **343,*** 105-116.

Stalker, J.R. and K.R. Knupp, 2002: A method to identify convective cells within multicell thunderstorms from multiple Doppler radar data, *Mon. Wea. Rev.*, **120**, 188-195.

Stumpf, G.J., A.E. Witt, E. D. Mitchell, P. L. Spencer, J. T. Johnson, M. D. Eilts, K. W. Thomas, and D. W. Burgess, 1998: The National Severe Storms Laboratory Mesocyclone Detection Algorithm for the WSR-88D. *Wea. Forecasting,* **13,** 304-326.

Thompson, R.L., R. Edwards, J.A. Hart, K. Elmore and P. Markowski, 2003: Close proximity soundings within supercell environments obtained from the rapid update cycle. *Wea. Forecasting,* **18**, 1243-1261.

Witt, A.E., M.D. Eilts, G. J. Stumpf, J.T. Johnson, E.D. Mitchell, and K.W. Thomas, 1998: An enhanced hail detection algorithm for the WSR-88D. *Wea. Forecasting,* **13,** 286–303.

Xu, K., C.K. Wikle, and N.I. Fox, 2005: A kernel-based spatio-temporal dynamical model for nowcasting weather radar reflectivities, *J. Am. Stat. Assoc*, **100**, 1133–1144.